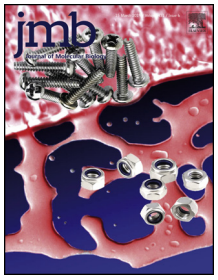

Optogenetic Navigation of Routes Leading to Protein Amyloidogenesis in Bacteria

Rafael Giraldo

Department of Cellular and Molecular Biology, *Centro de Investigaciones Biológicas—CSIC, c/ Ramiro de Maeztu 9, E28040 Madrid, Spain*

Correspondence to Rafael Giraldo: *Department of Microbial Biotechnology, National Centre of Biotechnology—CSIC, c/ Darwin 3, Campus Cantoblanco, E28049 Madrid, Spain.* *rgiraldo@cnb.csic.es*
https://doi.org/10.1016/j.jmb.2019.01.037
Edited by S. Koide

Abstract

Modulation of liquid–liquid and liquid–hydrogel phase transitions is central to avoid the cytotoxic aggregation of proteins in eukaryotic cells, but knowledge on its relevance in bacteria is limited. Here the power of optogenetics to engineer proteins as light-responsive switches has been used to control the balance between solubility and aggregation for LOV2–WH1, a chimera between the plant blue light-responsive domain LOV2 and the bacterial prion-like protein RepA-WH1. These proteins were first linked by fusing, as a continuous α-helix, the C-terminal photo-transducer Jα helix in LOV2 with the N-terminal domain-closure α1 helix in RepA-WH1, and then improved for light-responsiveness by including mutations in the Jα moiety. In the darkness and in a crowded solution *in vitro*, LOV2–WH1 nucleates the irreversible assembly of amyloid fibers into a hydrogel. However, under blue light illumination, LOV2–WH1 assembles as soluble oligomers. When expressed in *Escherichia coli*, LOV2–WH1 forms in the darkness large intracellular amyloid inclusions compatible with bacterial proliferation. Strikingly, under blue light, LOV2–WH1 aggregates decrease in size, while they become detrimental for bacterial growth. LOV2–WH1 optogenetics governs the assembly of mutually exclusive inert amyloid fibers or cytotoxic oligomers, thus enabling the navigation of the conformational landscape of protein amyloidogenesis to generate potential photo-activated anti-bacterial devices (optobiotics).

Introduction

Amyloids, which are among the most stable natural macromolecular structures, are made of β-strand segments from different individual molecules of a given protein that assemble, through intermediate oligomeric states, to form mature fibers [1]. Amyloidogenesis is readily accessible to short peptides or intrinsically disordered regions (IDRs) in proteins but, for domains with a stable three-dimensional fold, partial unfolding to a metastable state is mandatory. This is usually attained through disease-linked destabilizing mutations *in vivo*, or by resorting to harsh physical–chemical conditions *in vitro* [2]. Recently, liquid–liquid and liquid–hydrogel phase transitions have emerged as key regulators of the conformational and functional landscapes of proteins in eukaryotic cells [3], in particular for the IDRs in proteins that bind to RNA [4]. Interestingly, the irreversible shift of these protein phase transitions toward a solid state is a main physical–chemical basis for amyloidosis [5–8]. However, such transitions have not been characterized so far in the bacterial cytosol.

RepA-WH1 is a manifold domain from a plasmid-encoded bacterial protein that undergoes conformational changes [9] that capacitate it either as a transcriptional repressor, as a DNA replication initiator or, through its assembly as amyloid oligomers, to hinder premature re-replication rounds [10]. Although very stable in solution, RepA-WH1 dimers become metastable monomers upon allosteric binding to plasmid-specific dsDNA sequences [11–13], or acidic phospholipids [14], thus paving the way toward amyloidogenesis. The fusion of a hyper-amyloidogenic mutant variant of RepA-WH1 to the fluorescent protein mCherry generates a prion-like protein (prionoid) that is epigenetically transmitted from mother-to-daughter bacterial cells, causing a synthetic amyloid proteinopathy [15,16]. In the bacterial cytosol, RepA-WH1 aggregates propagate as two distinct strains, with the appearance of multiple globular, dense foci or a single comet-shaped, fluidized particle

that exhibit, respectively, acute or mild cytotoxicity. The Hsp70 chaperone DnaK is capable to drive the transformation of the globular into the comet-shaped particles [16]. RepA-WH1 amyloidosis recapitulates in bacteria some of the hallmarks of the mitochondrial route associated with human amyloid diseases, including the formation of oligomeric pores at the internal membrane, with a net decrease in ATP levels and the generation of reactive oxygen species, and the loss of function, due to co-aggregation, of stress-responsive cell factors [17]. In addition, RepA-WH1 has been used as a benchmark for the design of synthetic tools to probe protein amyloidogenesis, including gold nanoparticle-based sensors [18] and screening devices based on amyloid-promoted overriding of translation termination, either in yeast [19] or in bacteria [20].

The design of protein chimeras including a light-responsive photosensor domain has equipped Synthetic Biology with powerful optogenetic tools to get physical control on cellular processes [21]. Optogenetic parts have been successfully designed to govern ion fluxes across membrane channels and thus neuronal circuits, cytoskeleton dynamics and nuclear localization, membrane trafficking, allosteric photoregulation of enzyme catalysis, apoptosis through activating caspases, protein degradation by ubiquitinylation, or gene expression through regulation of the binding of proteins to DNA [22]. Photosensor domains, such as light-oxygen-voltage 2 (LOV2) in the plant phototropin 1 [23–25], upon illumination with light of a wavelength matching an absorption band in a chromophoric prosthetic group, undergo conformational changes that are coupled with a functional switch in a fusion partner, for example, an effector peptide tag becomes exposed [26]. Optogenetic approaches to modulate liquid–liquid and liquid–hydrogel phase transitions in proteins with IDRs have been recently developed [27,28]. However, to the best of the author's knowledge, no optogenetic tool has been described yet having direct control on the amyloidogenesis of any folded and stable protein domain.

Here the feasibility of using optogenetics to surf the conformational landscape and the phase diagram of a protein on a pathway leading to amyloidosis has been explored for the first time in bacteria by building a synthetic device (LOV2–WH1) that assembles in the darkness as a hydrogel made of amyloid fibers, while under blue light illumination forms soluble oligomeric particles that are cytotoxic.

Results

Design of LOV2–WH1 chimeras

The key determinant of RepA-WH1 stability is the formation of a “latch” by locking the C-terminal helix α5 in between the V-shaped folded N-terminal helices α1-α2, thus closing topologically the domain [9]. RepA-WH1 (in short, WH1) can be destabilized by mutating the inner hydrophobic spine in α1 (Leu12 to Ala and Leu19 to Ala) or by stretching the C-terminus of α5 through its fusion to the fluorescent probe mCherry [14–16]. The possibility to manipulate the stability of WH1 by straining this domain at its N-terminus has been explored here constructing a chimeric continuous α-helix between the C-terminal Jα helix in the *Avena sativa* phototropin domain LOV2 (Fig. S1a) [29], and α1 in WH1. Upon absorption of blue light photons (λ_{max} 447 nm) by the FMN chromophore in LOV2, Jα unfolds and detaches from the core of the domain [30,31], thus unconstraining the conformation of any sequence to which this helix had been intentionally linked [32–34].

Three different helical phases in the Jα–α1 linker, and thus three distinct relative geometrical arrangements of LOV2 and WH1, were constructed by PCR (Fig. S1b). The WH1 wild-type domain was used in the chimeras due to its higher solubility compared with some mutant variants (e.g., A31V, which is hyper-amyloidogenic) [11,15,35]. The constructs displayed both domains either at opposites sides (LOV540–WH1 and LOV543–WH1) or at the same side (LOV542-WH1) of the Jα–α1 helix (Fig. 1a). The difference between the former two chimeras is the length of the linker, being about a helical turn longer in LOV543–WH1 (4 extra amino acid residues; Fig. S1c) than in LOV540–WH1. As a first screening, the three chimeras were expressed in *Escherichia coli* with N-terminal His_{10} tags, either in the darkness or under illumination with blue light [using a custom-built light-emitting diode (LED) device; Fig. S2] and, upon cell lysis, their sedimentation behavior was tested (Fig. 1b). It turned out that only the LOV543–WH1 chimera was present to a substantial extent in the soluble fraction, albeit its solubility balance did not vary much between cell extracts from bacteria grown in the darkness or under blue light illumination. The insolubility of the other two constructs may reflect either blocking of the switch by a too tight package of the domains, due to the reduced length of the linker (in LOV540–WH1), or steric hindrance by the N-terminal LOV2 domain to proper folding of C-terminal WH1 (most likely in LOV542-WH1) (Fig. 1c). It is noteworthy that tuning the helical phase of Jα is a common requirement in optimizing the response to light of other synthetic LOV2 chimeras [25]. All subsequent experiments were thus performed with LOV543–WH1 (and its m3 mutant, described below).

Addressing light-responsiveness of LOV2–WH1 through limited proteolysis

Proteolysis is a probe for the accessibility to the solvent of target peptide sequences and thus for the stability of folded protein domains. Three residue-selective proteases were assayed on LOV543–WH1,

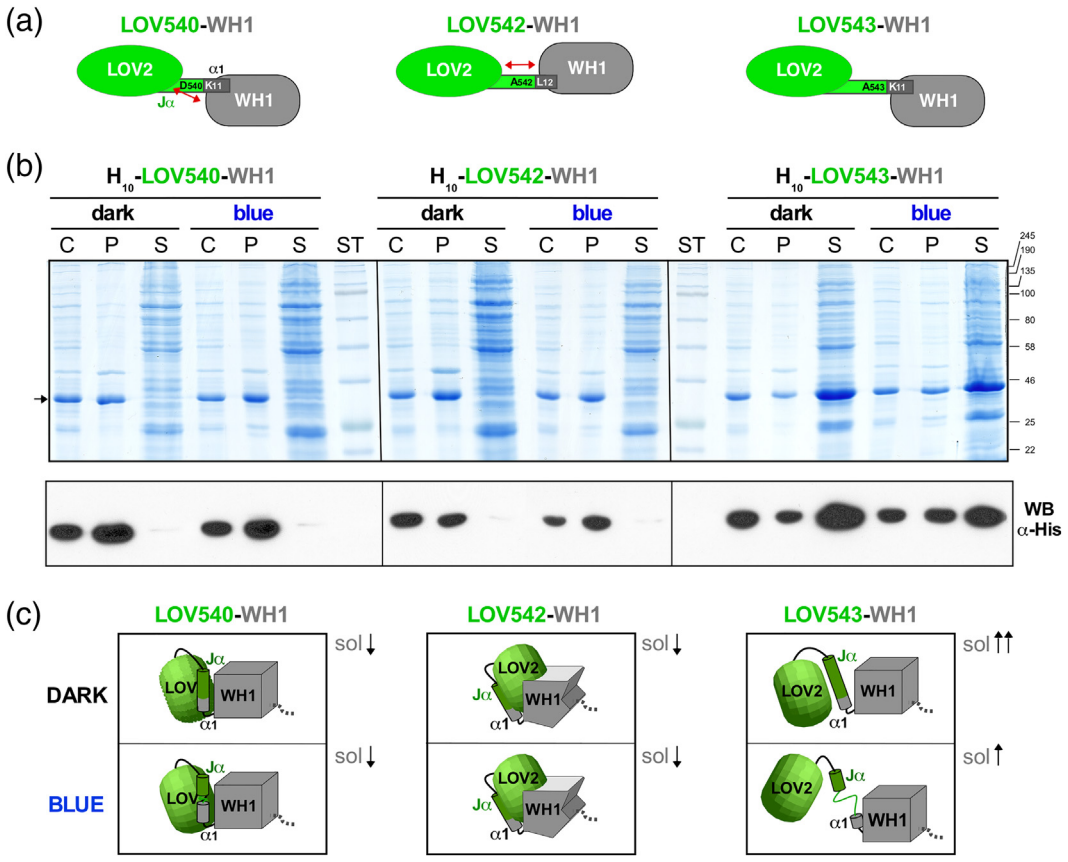

Fig. 1. Assessing the solubility of distinct helical phases for the Jα–α1 linker in LOV2-RepA-WH1 chimeras. (a) Schematic representation of the arrangement of the three chimeras assayed (Fig. S1). The linker helix increases its length by a helical turn between LOV540 (closest position related to WH1) and LOV543 (farthest to WH1), displaying both domains on opposite faces of the helix, whereas in LOV542 both are found on the same face and intermediate position. (b) Fractionation of bacterial cells (labeled as C) expressing the chimeras into the soluble (S) and insoluble (P) fractions (*top* panel), plus their detection by Western blotting (anti-His tag antibody; *bottom*). Only LOV543–WH1 generates a significant soluble fraction, with no major differences when cultures were carried out in the darkness or under blue light illumination. (c) These results are compatible with steric hindrance due to close apposition of the domains by a short linker (LOV540–WH1) and/or their mutual interference for folding (LOV542-WH1), whereas only LOV543–WH1 has the right disposition of both domains to fold independently.

either in the dark or under blue light illumination (Fig. 2a). Peptides were separated by SDS-PAGE, revealing that blue light enhanced the cleavage by chymotrypsin and V8 protease, which yielded two main protein bands whose sizes roughly corresponded to the expected for the individual LOV2 and WH1 domains. The identities of the fragments corresponding to the LOV2 and the WH1 domains were confirmed through peptide fingerprinting (Fig. S3). Trypsin generated multiple cleavage sites whose accessibility increased to lesser extent upon blue light illumination. N-terminal peptide sequencing was performed on the chymotrypsin and V8 digestions that had been incubated under blue light, allowing for the identification of the major cleavage sites for each protease in the LOV543–WH1 sequence (Fig. 2b). Cleavage sites, with the residue preference expected for each protease, were found precisely at the junction between Jα–α1, confirming that this helical linker became unfolded, as designed, upon illumination of the LOV543–WH1 chimera with blue light (Fig. 2c).

Improving the LOV2–WH1 switch by mutagenesis

A major concern in the design of any synthetic switch through protein fusion is how this affects the dynamic range of the device, that is, the net ratio between the response of a chimera to the ON and the OFF stimuli. In optogenetics, this ultimately reflects the balance between the fraction of molecules that remain in the OFF (pseudo-dark) state upon illumination and the fraction of molecules that populate the ON (pseudo-lit) state in the darkness [26,36]. A number of mutations at the Jα helix and its environment have been shown to consistently

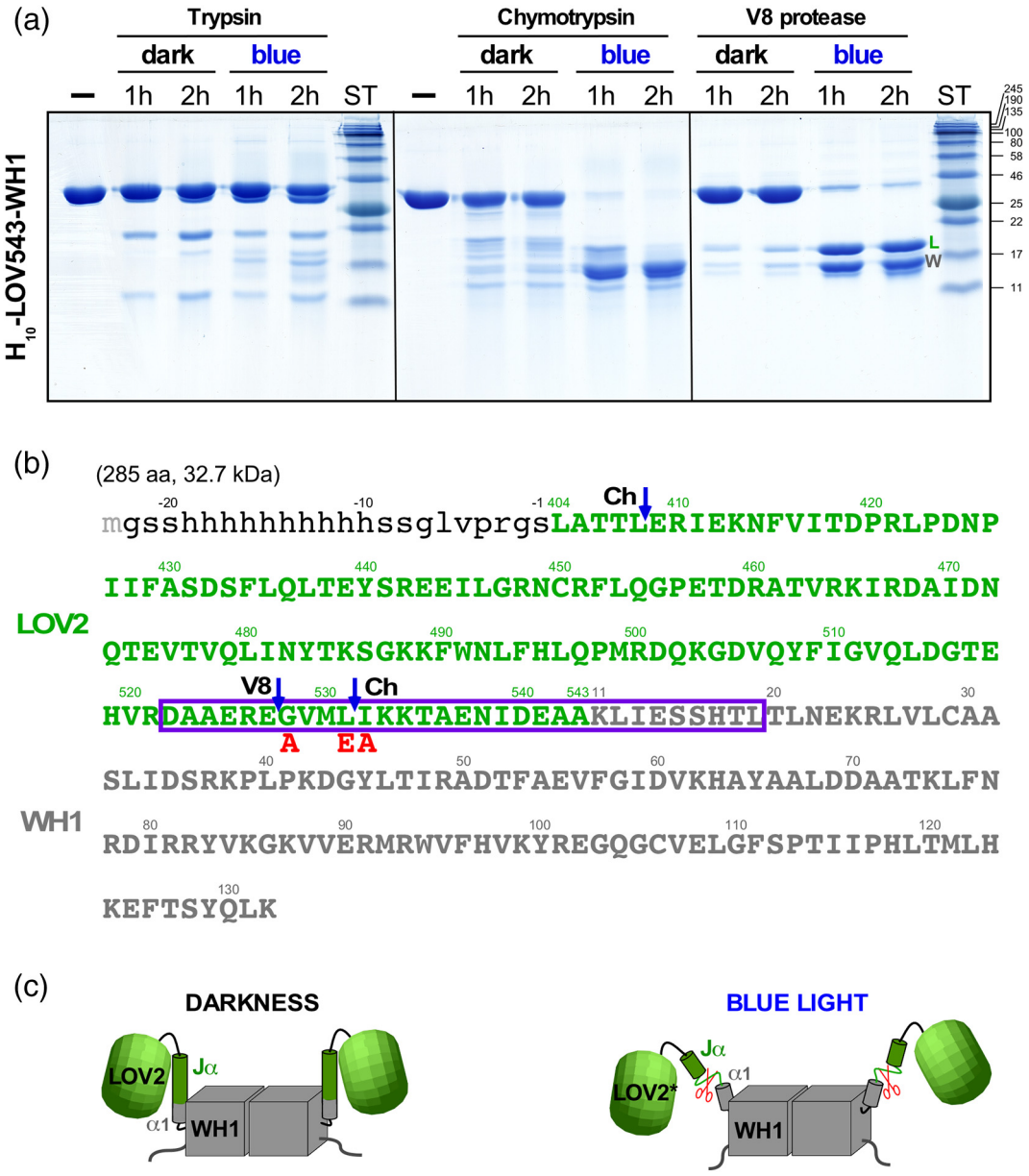

Fig. 2. Limited proteolysis reveals blue light remodeling of the Jα–α1 helical linker in LOV2–WH1. (a) SDS-PAGE of proteolytic digestions of LOV543–WH1. Cleavage sites for chymotrypsin (Ch) and V8 protease become accessible in the illuminated state, generating fragments as expected for LOV2 (≈17 kDa) and WH1 (≈15 kDa) (on their identification, see Fig. S3). (b) Sequence of the LOV543–WH1 protein fusion. Residue numbers are from *As*LOV phototropin (green) and RepA (gray). N-terminal sequencing of the fragments identified unambiguously the cleavage sites (arrows) for chymotrypsin (I_{532}KKTA and E_{409}RIEK) and V8 protease (G_{528}VMLI). The N-terminal Met was removed *in vivo*, leaving the H_{10}-tag (lower case). The Jα–α1 linker helix is boxed (magenta), with the three residue changes in LOV543m3–WH1 (Figs. S4 and S5) typed in red. (c) Schematic representation of the detachment and unfolding of the chimeric Jα–α1 helix upon blue light illumination, which increase its accessibility to proteases (scissors).

improve the dynamic range for LOV2 fusions [24,25,33,34]. Three of them were introduced in LOV543–WH1 to generate LOV543m3–WH1 (Fig. S4): I532A [33], G528A [33], and L531E [37], which are known to improve, in the dark state, the packing of the N-terminus of Jα with the backing β-sheet in LOV2. The structure of the LOV543m3–WH1 chimera was modeled on the PDB coordinates of its two component domains using the *Rosetta* structure prediction method [38]. Figure S5a displays a high-score *in silico* model supporting the structural feasibility of the three mutations within the fully folded chimera, which showed no stereochemical violations (Fig. S5b).

The LOV543wt–WH1 and LOV543m3–WH1 fusions were expressed in *E. coli*, purified and characterized through biophysical approaches (Fig. 3). Measurements of the return to the dark state after saturating blue-light stimulation, by following the evolution of the absorption spectra of the FMN group (band at 447 nm) [34,39], indicated a 3-fold increase in the half-life of the excited state ($\tau_{1/2}$) for the m3 mutant (16.7 s) compared with its parental wt protein (5.6 s) (Fig. 3a). These $\tau_{1/2}$ values are notably shorter than those typical for wild-type LOV2 (80 s) [34], probably reflecting the burden to the docking of Jα imposed by its fusion, through α1, to the α1–α2–α5 latch in WH1 [33]. No significant differences between the wt and m3 chimeras were observed concerning the association state of the proteins, which remained essentially dimeric as indicated by gel filtration analyses performed either in the darkness or under continuous blue light illumination (Fig. 3b). The higher solubility of the LOV543m3–WH1 chimera facilitated to confirm its dimeric state by sedimentation velocity analysis carried out in two ultracentrifuge cells filled with the protein and set-up for optical radial scanning at 275 nm (pseudo-dark) and at 450 nm (blue light), respectively (Fig. S6a). This observation suggests that in the chimera, dimerization continues to be dictated by the stable antiparallel β-sheet interface in RepA-WH1 [9]. Strikingly, LOV543wt–WH1 aggregated massively on any attempt to either freeze or concentrate it beyond 6 μM, while LOV543m3–WH1 withstood storage in a frozen state at ≥10-fold concentrations. Circular dichroism (CD) spectra of both chimeras in the darkness showed the typical α-helical profile, with a more pronounced negative band at 208 nm for the m3 chimera (Fig. 3c, left). This is an indication for an increase in the length of α-helices [40], as expected from the stabilization of Jα in the dark state by the three mutations engineered in LOV543m3–WH1. Thermal denaturation analyses (Fig. 3c, right) indicated that both chimeras were stable, showing a single irreversible transition between two states (folded and unfolded) with a T_m (50% unfolding) of 57 °C (Fig. 3c, right).

Light modulates the capacity of LOV2–WH1 to cross-seed RepA-WH1(A31V) amyloidogenesis

Seeding, that is, the ability of a pre-formed amyloid aggregate to template and nucleate amyloid growth from soluble molecules of the same (or a closely related) protein, is a hallmark of amyloidogenesis [2]. To test the capacity of LOV543–WH1 to act as a light-controlled seed, substoichometric amounts of the purified chimeras (either the wt or m3 variants) were supplied to an excess of soluble RepA-WH1(A31V) (Fig. 4a). This is a hyper-amyloidogenic RepA-WH1 variant that efficiently assembles into fibers *in vitro* [11,41], provided that a nucleation agent, such as purified RepA-WH1(A31V) aggregates preformed *in vivo* [15], is supplied as seeds.

The formation of RepA-WH1(A31V) fibers was thus explored, either under continuous blue light illumination or in the darkness, by transmission electron microscopy (TEM) (Fig. 4b), thioflavin-S (ThS) fluorescence emission, and Congo red (CR) birefringence under polarized light (Fig. 4c). The results of these assays indicated that just spare amorphous aggregates were found in the absence of any supplied seed, while fibers were the product of nucleation by the intracellular RepA-WH1(A31V) aggregates, as previously reported [11,15,41]. Interestingly, similar fibril aggregates were generated upon the addition of LOV543wt–WH1, but no differential fibrillation response to the darkness/blue light regimes was observed for this chimera. On the contrary, the LOV543–WH1m3 variant nucleated on RepA-WH1 (A31V) the formation of neat fibrils in the darkness, but of discrete drop-like particles and thin needles under blue light (Fig. 4b). When compared to the mature fibers, the blue light-promoted species have much reduced amyloid character, according to both ThS and CR staining (Fig. 4c). Because only the LOV543m3–WH1 chimera was able to modulate the fiber/oligomer balance in the assembly of RepA-WH1 *in vitro* under selective conditions (i.e., darkness/blue light), this protein fusion was selected to further explore its capability to build complex supramolecular assemblies.

LOV543m3–WH1–mCherry enables optogenetic control on a liquid–hydrogel phase transition

To visualize the effect of darkness *versus* blue light illumination on LOV543m3–WH1 aggregation, both *in vitro* and *in vivo*, the monomeric red fluorescent reporter protein mCherry was fused to the C-terminus of the WH1 domain (Fig. S7). It is noteworthy that the fusion to mCherry does not alter by itself the dimeric association state of RepA-WH1 *in vitro* [14] or its solubility *in vivo* [15,35]. The LOV543m3–WH1–mCherry protein was then purified and characterized through several biophysical approaches (Fig. 5). The half-life of the excited state, measured as the recovery of the absorption band at 447 nm after transferring pre-illuminated samples to the darkness [34,39], was improved by 2.3-fold (to 38.3 s) compared to the LOV543m3–WH1 fusion, with the decoupled mCherry band (at 586 nm) dominating the spectra and showing no temporal variation (Fig. 5a). As it was shown for its parental double chimera (Fig. 3b, right), according to gel filtration (Fig. 5b) and sedimentation velocity (Fig. S6b) analyses, LOV543m3–WH1–mCherry remained as a dimer either in the darkness or under blue light. The CD spectrum (Fig. 5c) was much dominated by the β-sheet structure of mCherry, which also imprinted thermal stability (T_m = 85.5 °C). However, as for the LOV543wt/m3–WH1 fusions,

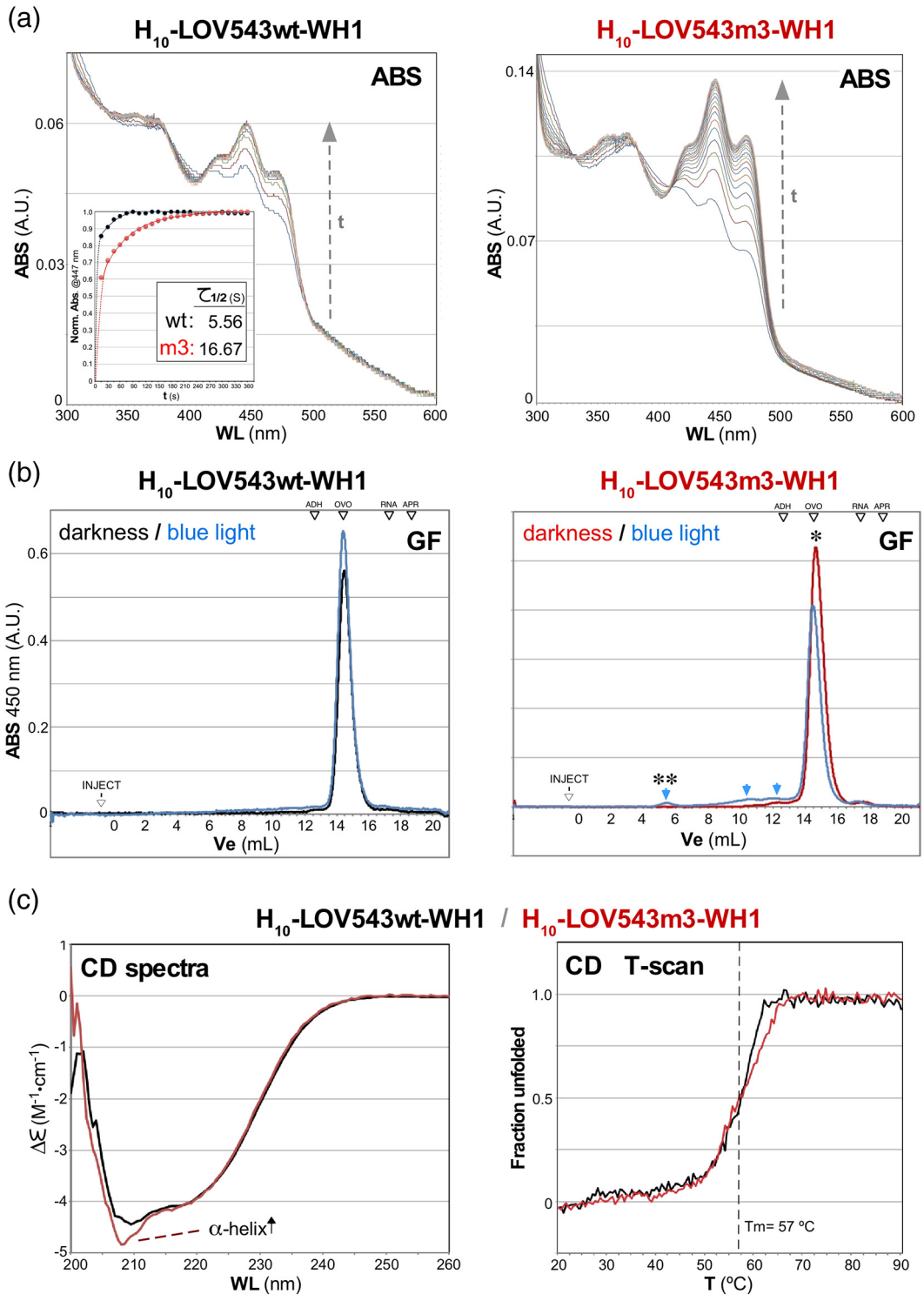

Fig. 3. Biophysical characterization of LOV543wt–WH1 (*left* column) and LOV543m3–WH1 (right). (a) Absorption spectra showing a time course of the return of the blue light-excited chimeras to the ground (dark) state. Spectra were acquired with 15-s intervals after switching the blue LEDs off and then plotted overlaid. Inset: kinetics of the return to the ground state, measured as the value of the absorption band at 447 nm for each spectrum. Curves display double exponential function fittings to the data points. $\tau_{1/2}$: half-life of the lit state. (b) Gel filtration elution profiles of the purified chimeras, run in the darkness or under continuous blue light illumination. The major species correspond to protein dimers, in spite of having been illuminated or not, as it was confirmed, for LOV543m3–WH1, through sedimentation velocity analyses (Fig. S6a). Arrows point to minor oligomeric species. MW standards: aprotinin (APR), RNase A (RNA), ovoalbumin (OVO) and alcohol dehydrogenase (ADH). (c) CD spectra (left) and thermal denaturation profiles (right) of the purified chimeras.

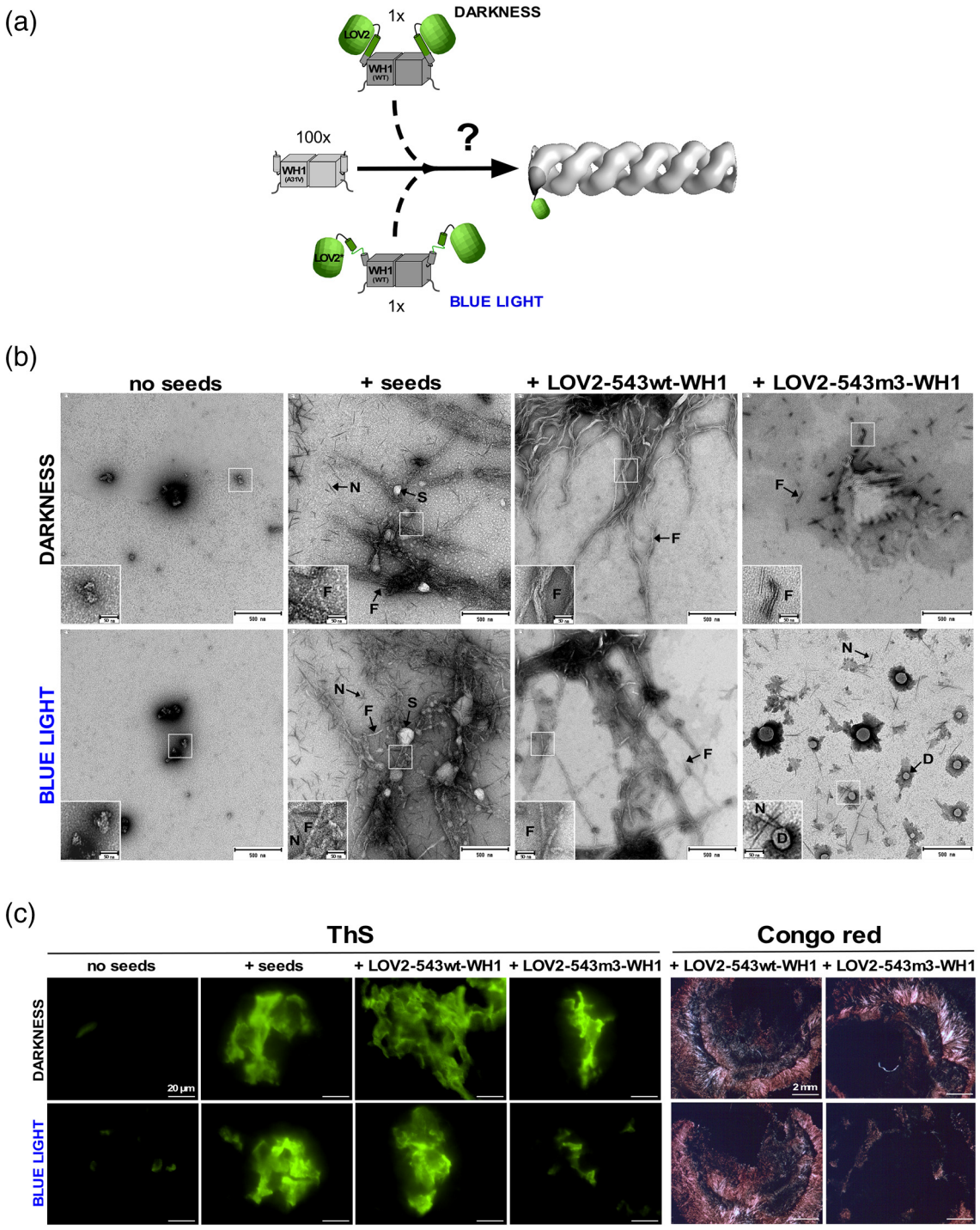

Fig. 4. *In vitro* assembly of RepA-WH1(A31V) amyloid fibers cross-seeded by LOV543wt/m3–WH1. (a) Outline of the experiment. RepA-WH1(A31V) and the assembled fibers [41] depicted in light gray, LOV2–WH1 as in Fig. 2c. (b) TEM of the aggregates generated upon incubation of RepA-WH1(A31V) with the optogenetic seeds (100:1). Control samples: un-seeded and RepA-WH1(A31V)–mCherry seeds purified from *E. coli* (labeled as S). LOV543wt–WH1, whether illuminated or not, templates on RepA-WH1(A31V) the assembly of fibers (F). LOV543m3–WH1 seeds the growth of shorter fibers (darkness) or an ensemble of needles (N) and spherical/drop-like particles (D) (blue light). Magnification: 20,000× (insets: 50,000×). (c) Fluorescence emission (ThS, *left*) and optical birefringence (CR, *right*). ThS and CR bind to the amyloid aggregates templated by the control seeds or by LOV543wt–WH1, while the particles seeded by LOV543m3–WH1 under blue light are bound weakly.

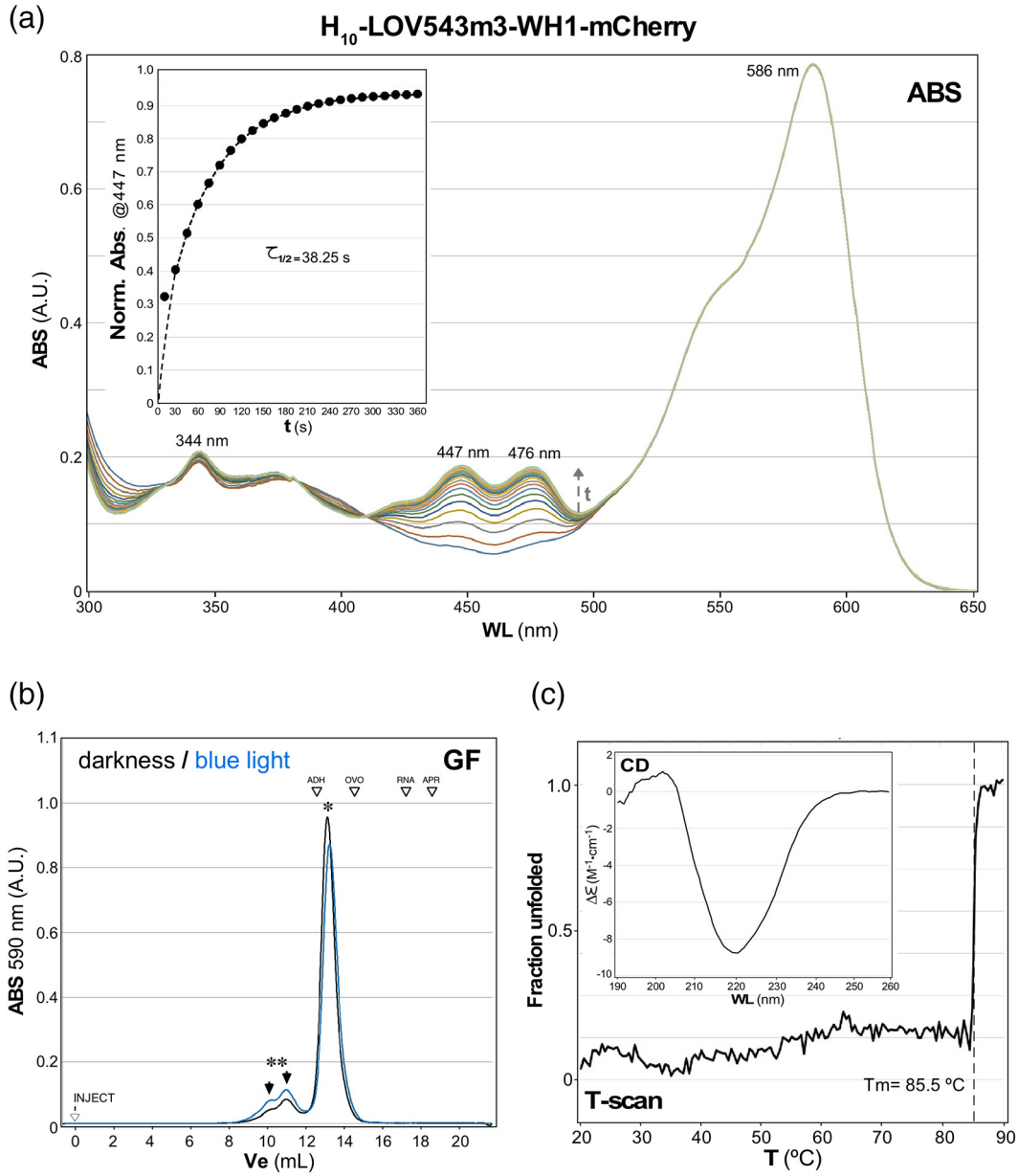

Fig. 5. Biophysical characterization of the LOV2m3-WH1–mCherry chimera. (a) Absorption spectra displaying the return of the blue light-excited chimera to the ground (dark) state. Spectra were acquired with 15-s intervals after switching the blue LEDs off. Inset: kinetics of the recovery of the dark state (see Fig. 3), measured as the value of the absorption band at 447 nm for each spectrum. Curve shows a double exponential fitting for the data points. $\tau_{1/2}$: half-life of the lit state. (b) Gel filtration elution profiles of the purified chimeras, run in the darkness or under continuous blue light illumination. The major species corresponds to a protein dimer (single asterisk), as confirmed by sedimentation velocity profiles (Fig. S6b). Arrows and double asterisks point to minor oligomeric aggregated species. (c) CD thermal denaturation profile. Inset: CD spectrum.

these assays were carried out under ideal (diluted) buffer conditions, not attempting to mimic the crowded environment of the bacterial cytosol.

The assembly potential of LOV543m3–WH1–mCherry was then tested *in vitro* at a very high protein concentration (0.25 mM), in a low-salt buffer and in the presence of polyethylene glycol (PEG) 4000, a crowding agent that enhances RepA-WH1 fibrillation (Fig. 6) [11]. In the darkness, the triple chimera decanted to the bottom of the test tubes, clearly separated from the buffer supernatant, with the visual appearance of a hydrogel (Fig. 6a). TEM showed the coexistence within the hydrogel of spherical particles and tightly packed fibril bundles (Fig. 6b). On the contrary, when samples were continuously illuminated with blue light, they stayed as a transparent solution (Fig. 6a) that included,

as revealed by TEM, ring-like oligomers (Fig. 6b). Exploring with time-elapsed epifluorescence microscopy such liquid-to-hydrogel phase transition for LOV543m3–WH1–mCherry confirmed that, as long as samples were illuminated with blue light (up to 24 h), the protein remained liquid, including mobile entrapped micro-droplets. Interestingly, when turned into the darkness, the protein solution evolved within ≥1 h into a thick hydrogel with the appearance of a sponge that, according to the enhancement in the emission of ThS fluorescence, had amyloid nature (Fig. 6c). Darkness-promoted gelation of LOV543m3–WH1–mCherry was not reversible.

LOV543m3–WH1–mCherry is an optogenetic switch for bacterial growth

Expression in *E. coli* of the LOV543m3–WH1 (WT)–mCherry triple chimera in the darkness resulted in the appearance of cytosolic red fluorescent

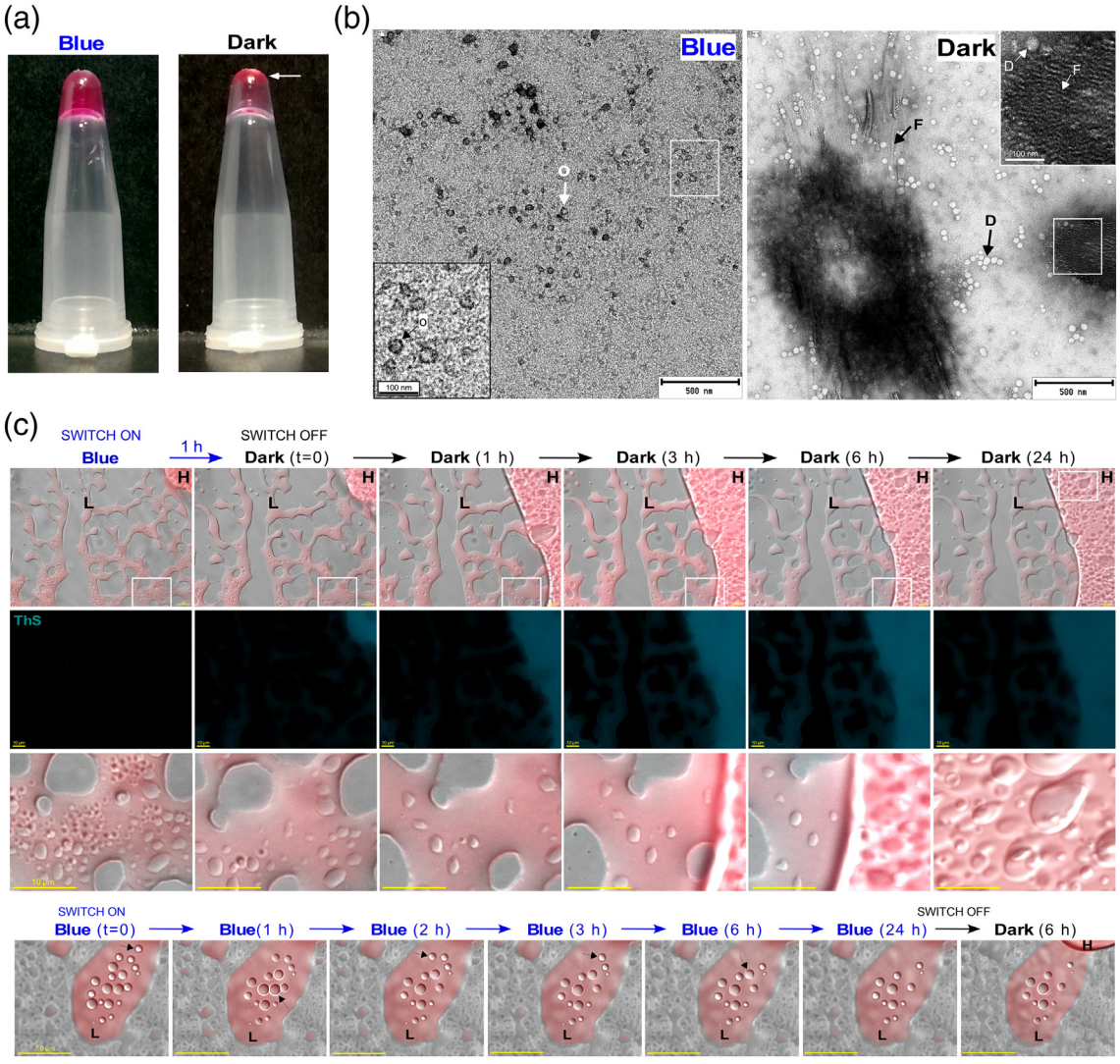

Fig. 6. Optogenetics triggers a liquid-to-hydrogel phase transition in LOV2–WH1–mCherry. (a) LOV543m3–WH1–mCherry in a crowded solution and in the darkness forms a clearly separated gel phase at the bottom of the tubes (arrow), whereas blue light illumination keeps the protein soluble. (b) TEM. The hydrogel formed in the darkness is made of a mixture of tightly packed fibers (labeled as F) and spherical, drop-like particles (D), whereas the liquid phase under blue light contains discrete annular oligomers (o). Magnification: 20,000× (insets: 50,000×). (c) Epifluorescence visualization of a time course (24 h) gelation experiment (upper panel). Samples were assembled under blue light and then transferred to the darkness. Superimpositions of DIC and TRITC (mCherry) channels (top row), or the fluorescence from ThS (middle row) are displayed. The boundary between the liquid (L) and the expanding hydrogel (H) phases is evident. Bottom row: zoom (5×) of the sectors boxed above. Lower panel: a control time course carried out under continuous blue light illumination. The liquid nature of the protein is evident from the successive displacement out of the focal plane of the inclusions market with arrows.

amyloid protein inclusions, stainable with ThS (Fig. 7a, left). These were very much alike the aggregates reported for the prion-like, hyper-amyloidogenic A31V variant of RepA-WH1 fused to mCherry, rather than as for its soluble parental (WT) protein fusion [15,16,35]. However, such aggregates were fewer and with lower affinity for ThS (i.e., ≈1/3 fluorescence intensity) in cells grown under blue light (Fig. 7a, right). Quantitation of these aggregation phenotypes in bacterial populations (Fig. 7b) indicated that 37% of them exhibited intense ThS-stainable protein aggregates in the darkness. On the contrary, if expression of LOV543m3–WH1–mCherry was carried out under blue light illumination, just 4% of the cells showed ThS fluorescence emission. Essentially none of the bacterial cells expressing LOV543m3–mCherry, a control protein lacking WH1 (Fig. S7a, b), presented cytosolic aggregation, neither in the darkness nor under blue light illumination (Fig. S8). This was expected due to the absence in LOV543m3–mCherry of an amyloidogenic domain. Furthermore, a significant increase in size and filamentation of the bacterial cells expressing LOV543m3–WH1–mCherry in the darkness was also evident, but not in the population expressing the LOV543m3–mCherry control (Fig. 7c). This is a phenotype characteristic of RepA-WH1 (A31V)–mCherry expression but not of RepA-WH1 (WT)–mCherry [16,35], suggesting that LOV2 indeed destabilizes the fold of the native RepA-WH1 turning it into amyloidogenic. Biochemical analysis of the solubility of the triple chimera upon cell lysis and subsequent sedimentation plus Western-blotting (Fig. 7d) confirmed that the fraction of LOV543m3–WH1–mCherry in the supernatant increased in cultures illuminated with blue light (59%) compared with those grown in the darkness (23%).

To survey a possible effect of the optogenetically-regulated expression of LOV543m3–WH1–mCherry on bacterial proliferation, serial dilutions of exponential phase *E. coli* cultures that had been grown in the darkness were plated on LB-agar including (or not) the inducer IPTG (Fig. 7e). While in the absence of expression of the triple chimera, or upon expression of the control protein LOV543m3–mCherry, no difference was appreciated between drops incubated in the darkness or under blue light illumination, LOV543m3–WH1–mCherry expression reduced by ≥100-fold the growth of bacterial colonies under blue light when compared to darkness incubation. Cultures carried out in liquid LB medium also showed a market slowing down in growth, and a reduction in the maximum cell density, for bacteria expressing LOV543m3–WH1–mCherry under blue light illumination when compared to both growth in the darkness and, specially, to the LOV543m3–mCherry control (Fig. 7f). Because the presence of WH1 is the only differential element between LOV543m3–WH1–mCherry and its control, the strong inhibitory effect of the optogenetic switch in its lit state is attributable to RepA-WH1. Since blue light illumination promoted *in vitro* the assembly of oligomers of either LOV543m3–WH1 (Fig. 4) or LOV543m3–WH1–mCherry (Fig. 6), and amyloidogenic RepA-WH1 (A31V)–mCherry oligomers are the most cytotoxic molecular species of *in vivo* [17], oligomerization of the triple chimera through WH1 likely is at the basis for the observed decrease in *E. coli* growth under blue light.

Discussion

The absorption of photons by prosthetic groups has the capacity to elicit conformational re-arrangements in photoreceptor proteins. Optogenetics has implemented photoreceptor engineering to create synthetic conformational switches that much expand the functional abilities of proteins [21,22,26]. One of the most used switches in optogenetics is the LOV domain, with many variants widespread across the whole phylogenetic tree [42]. In this report, I describe a new kind of optogenetic device: a fusion between the plant phototropin domain LOV2 [24–26] and the bacterial domain RepA-WH1. LOV2 enables navigation through the folding landscape of RepA-WH1 from solubility to its aggregation as oligomers or amyloid fibers and hydrogels. RepA-WH1 naturally acts as a manifold switch between transcriptional repression, DNA replication initiation, and, finally, replication inhibition through the assembly of an amyloid oligomeric nucleoprotein complex that inhibits premature re-initiation [9,10]. RepA-WH1 was previously engineered to boost amyloidogenicity and uncouple conformational remodeling from its natural function, thus generating a unique intracellular amyloid proteinopathy in bacteria, which has been useful as a minimal model to deconstruct a “generic amyloid disease” [11,14–17].

LOV2–WH1 chimeras were optimized regarding the phasing and length of the Jα–α1 linker (Figs. 1 and S1), followed by the inclusion of mutations known to stabilize the dark state conformation of Jα (Figs. S4 and S5) [34,37]. The stiff Jα–α1 helix (Fig. 2) would thus act as a lever, unleashing the three-helix bundle (α1–α2–α5) that locks the fold of WH1 [9] and enabling the protein to template the assembly of amyloid fibrils (Fig. 4). On the contrary, under blue light illumination, the unfolding of the Jα–α1 linker (Fig. 2) would result in a conformational ensemble templating the assembly of distinct needle- or drop-shaped particles (Fig. 4).

The expression in *E. coli* of a triple chimera of LOV543m3–WH1 with mCherry led to the amyloid aggregation of a large fraction of the protein when bacteria were cultured in the darkness, whereas the soluble fraction increased in bacteria grown under blue light illumination (Fig. 7a–d). The C-terminal fusion to mCherry extends the half-life of the lit state of LOV2–WH1. This is probably due to the temporal

extension of the unfolding of the linker Jα–α1 helix as a consequence of mCherry-elicited stretching of α5, which would populate a partially open conformation of the α1–α2–α5 latch.

The discrete particles assembled *in vivo* by the triple chimera under blue light illumination exhibit a cytotoxicity greater than the large aggregates generated in the darkness (Fig. 7e, f), as previously reported for the RepA-WH1(A31V)–mCherry oligomers [14,20]. Comparing the *in vivo* behavior of both variants, RepA-WH1–mCherry requires the hyper-amyloidogenic mutation A31V in WH1 to become cytotoxic [15,17,20], while blue light illumination of the triple fusion including LOV2 is able to generate proteotoxic particles from the otherwise harmless wild-type WH1. Therefore, light-modulated conformational remodeling of the LOV543m3–WH1 chimeras is a reliable approach to gain control on RepA-WH1 amyloidogenesis and toxicity, either *in vitro* or *in vivo*.

The triple chimera LOV543m3–WH1–mCherry, albeit highly soluble *in vitro* (Figs. 5b and S6b), can be driven to aggregate as a hydrogel when in a crowded milieu and in the darkness, whereas it forms small soluble oligomers within a liquid phase when illuminated with blue light (Fig. 6). The affinity for ThS and the irreversibility of assembly of the LOV543m3–WH1–mCherry hydrogel, which is made of a mesh of laterally packed protein fibrils and oligomers, are indications of its amyloid nature. Liquid–liquid and liquid–hydrogel phase separations, a trendy topic in cellular biology, have been described for eukaryal RNA binding proteins including low-sequence complexity stretches, commonly found within IDRs [3–8]. Phase transitions may also be constituent players of the physiology of bacteria, since the bacterial cytosol experiences a glass–liquid transition upon activation of metabolism [43]. It is noteworthy that while RepA-WH1 is a folded, highly stable domain [9,11], in the bacterial cytosol the Hsp70 chaperone DnaK is able to remodel compact and toxic aggregates of RepA-WH1 (A31V)–mCherry to generate an elongated particle with a fluidized appearance and limited cytotoxicity [16]. In human cells, Hsp70 chaperones keep SOD1 (a folded protein involved in amyotrophic lateral sclerosis) in the liquid phase of stress granules, which would otherwise evolve into proteotoxic aggregates [44]. Therefore, not just proteins including IDRs can undergo phase transitions but also stably folded proteins, provided that a mechanism (e.g., binding to a polymeric allosteric ligand or to chaperones, post-translational modifications) promotes structural metastability and transient interactions [45]. Optogenetics has recently shown its potential to control phase separations when engineered into IDRs [27,28]. However, amyloid optogenetics with stably folded protein bacterial precursors remained yet unexplored.

LOV2–WH1 enriches the catalog of available optogenetic tools [21] with a novel way to navigate the conformational landscape of proteins toward amyloidogenesis. Engineering amyloids is now becoming a versatile constructive bio-resource [46,47]. In this sense, the potential applications of LOV2–WH1 optogenetics in bacteria may include, among others: controlling the assembly of amyloid nanoscaffolds to engage enzymes in sequential reaction steps; building transcriptional switches for synthetic gene expression circuits and light-controlled plasmid replication cassettes or the selective elimination of particular cells within a consortium, once they have fulfilled their task in a bioprocess. The development of a completely new kind of antimicrobials might be a focus of special attention. Such "optobiotics" would be based on triggering amyloidosis in the recipient bacterial cells upon horizontal gene transfer of mobilizable plasmids or prophages encoding light-switchable cytotoxic amyloids.

Materials and Methods

Construction of the LOV2–WH1 chimeras

The *AsLOV2* gene was custom-synthesized at ATG: biosynthetics (Merzhausen, Germany), with its codon composition optimized to the usage in *E. coli* (Fig. S1a). The template source of *repA-WH1* was pWH1(WT) [11]. Both genes were independently amplified by PCR using *Pfu* DNA polymerase (Fig. S1b, c), in such a way that in a subsequent PCR, an equimolar mixture of the *LOV2* and *repA-WH1* amplicons could hybridize through their tailored Jα-3′ and 5′-α1 encoding ends, respectively. Three alternative pairs of these linker primers were designed to generate three distinct fusions between both domains, and thus three distinctly phased chimeras: LOV_{540}–$WH1_{12}$, LOV_{542}–$WH1_{12}$, and LOV_{543}–$WH1_{11}$. The amplified chimeric fragments were then cloned into pRG-P_{tac}-His_{10} [48], through treatment with SacII and HindIII, plus T4 DNA ligase. LOV543m3–WH1 was generated on pRG-P_{tac}-His_{10}–LOV543wt–WH1 through two consecutive PCR reactions using the complementary annealed primers that included the mutations shown in Fig. S4a.

The LOV2m3–WH1–mCherry chimera, and its ΔWH1 control LOV2m3–mCherry, were built using pRG-P_{tac}-His_{10}–LOV543m3–WH1 and pRG-P_{tac}–His_6–mCherry [35] as templates for PCR amplification (with the primers described in Fig. S7a, b). The products, once digested with SpeI and HindIII, were cloned into pRK2-P_{tac}-His_{10} + $lacI^q$, a derivative of the low copy-number vector pSEVA121 [35,49] (Fig. S7c). All constructs were verified through DNA sequencing (Secugen, Madrid).

Protein expression and purification

The RepA-WH1(A31V) protein used in the fibrillation studies was purified as described [11]. The

LOV2–WH1 chimeras (H_{10}-LOV543wt/m3–WH1 and H_{10}-LOV543m3-WT–mCherry) were expressed in the *E. coli* strain BL21, in the presence of a helper plasmid providing T7 lysozyme to facilitate cell lysis. Three fourths of 1 L of Terrific Broth medium supplemented with ampicillin to 100 μg mL^{-1} (Ap_{100}) was inoculated with colonies from overnight LB agar plates with Ap_{100} and chloramphenicol to 30 μg mL^{-1} (Cm_{30}) and grown at 37 °C to an $OD_{600nm} \approx 0.8$. Then, IPTG was supplied to 1.0 mM, and the flasks were covered with aluminum foil. Expression proceeded for 5 h at room temperature (RT). Cells were harvested,

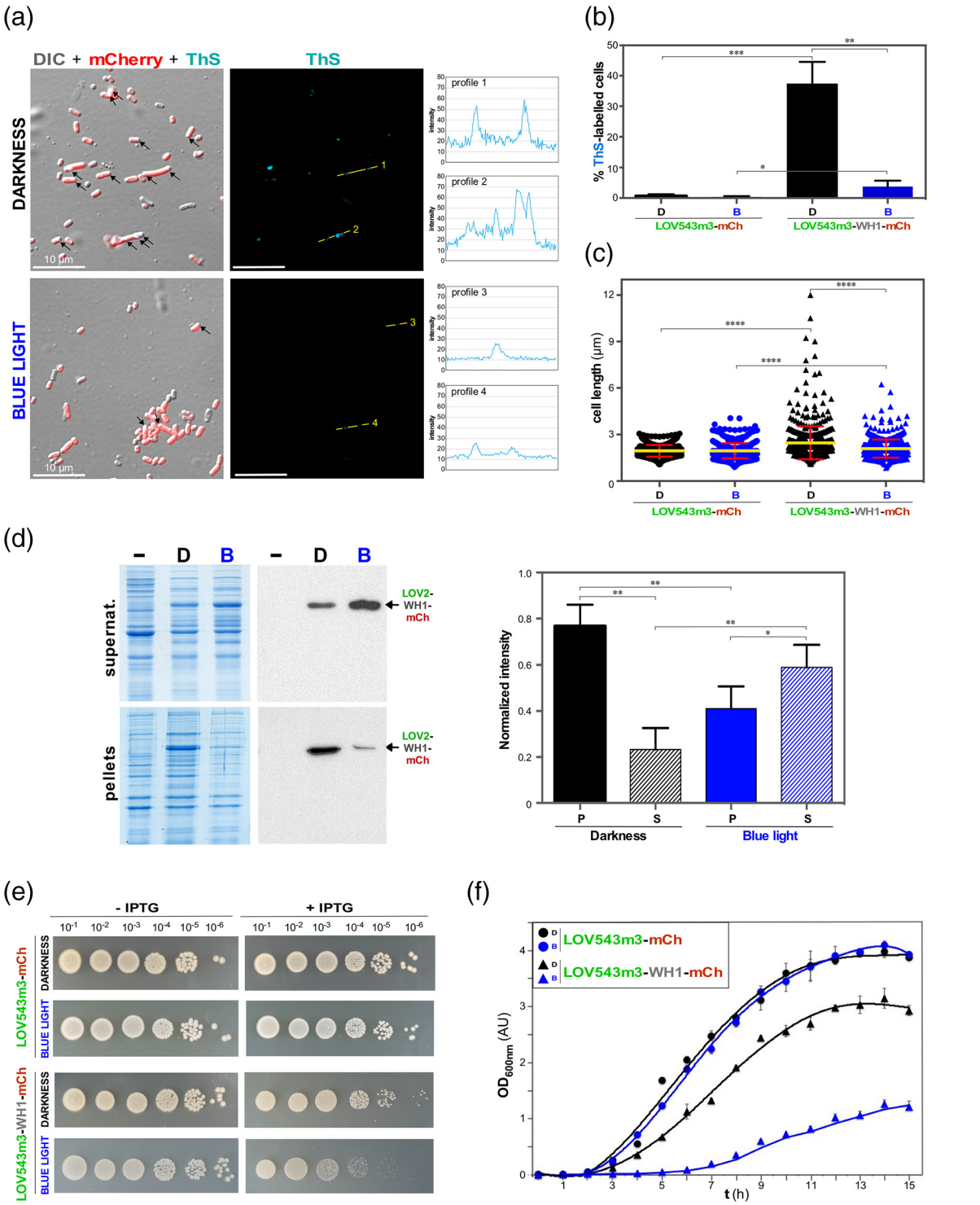

Fig. 7 (*legend on next page*)

washed with cold 0.9 NaCl, and resuspended in 15 mL of lysis buffer [0.5 M NaCl, 0.05 M imidazole (pH 8.0), 1% Brij-58, 10% glycerol, plus 1 pill of EDTA-free Roche protease inhibitors]. Cell suspension was frozen at −70 °C.

Cell lysis was enabled by thawing the cell suspension, and a clarified lysate was obtained by ultracentrifugation at 62,000*g* for 1 h at 4 °C. Supernatant was distributed in two aliquots, and each one was independently loaded into a Ni-affinity 5 mL (Agarose Beads Technologies) cartridge wrapped in aluminum foil and coupled to an ÄKTA basic 10 FPLC (GE Healthcare). After an extensive wash with column buffer A [0.5 M NaCl, 0.05 M imidazole (pH 7.8), 10% glycerol], a 25-mL linear gradient was run between this buffer and column buffer B [0.5 M NaCl, 0.75 M imidazole (pH 7.8), 10% glycerol]. Peak fractions were pooled and stored at 4 °C. Further purification was achieved by size-exclusion chromatography (SEC). SEC implied buffer exchange, required to eliminate imidazole, which otherwise would accelerate the return of the photo-activated LOV2 to the dark state [34]. SEC was carried out in a Superdex HR-200 column (GE Healthcare) equilibrated and run at 0.4 mL min^{-1} in SEC buffer [0.05 M Na_2SO_4, 0.010 M Hepes·NaOH (pH 7.6), 0.1 mM EDTA]. Peak elution profiles were monitored at A_{280}, A_{447}, and, for the chimera with mCherry, A_{590} nm.

Protein concentration was determined by absorption at 280 (RepA-WH1; ε = 11,548 M^{-1} cm^{-1}), 447 (H_{10}-LOV543wt/m3–WH1; ε = 13,800 M^{-1} cm^{-1}), or 590 (H_{10}-LOV543m3–WT-mCherry; ε = 70,700 M^{-1} cm^{-1}) nm. Protein chimeras were stored at 4 °C in the darkness for up to 2 weeks.

Protein solubility assays

Solubility of the chimeras, expressed in the *E. coli* K-12 reduced genome strain MDS42 [50], was assayed in whole cell lysates from 15 mL of cultures grown at 37 °C in LB plus Ap_{100}. When bacterial cultures reached OD_{600nm} = 0.2, IPTG was added to 0.5 mM and they were split into two aliquots, to be grown either in the darkness or under blue light illumination (1070 lux; Fig. S2). After 4 h of induction, cells were harvested and resuspended in 0.2× lysis buffer (see above), at a ratio of 0.33 mL per each unit of optical density (1.5×10^9 cells). EDTA (to 1 mM) and lysozyme (to 1 μ mL^{-1}) were supplemented and incubation proceeded for 15 min at RT. Cell lysates were centrifuged at 16,100*g* for 1 h at 4 °C, and the supernatant and pellet fractions were carefully separated.

Both fractions were then analyzed by SDS-PAGE (12.5% polyacrylamide gels), loading equal volumes of each supernatant and its corresponding pellet, resuspended in the same volume of loading buffer than its starting whole cell extract. Samples were run in duplicate: one set for Coomassie blue staining and the other for Western blotting. Transference to PVDF membranes was carried out by semi-dry blotting, followed by blocking in TTBS plus powder milk, as described [51]. Primary antibodies were used at 1:20,000 dilution, either mouse anti-His (Sigma) or rabbit anti–mCherry (Abcam), then incubated with HRP-conjugated secondary anti-mouse/rabbit antibodies at 1:20,000 (Sigma). Antibody binding was detected using the ECL 2 substrate (Pierce-Thermo).

Biophysical characterization of the H_{10}-LOV543wt/m3–WH1 and H_{10}-LOV543m3–WH1–mCherry chimeras

The photocycle of the FMN chromophore in the H_{10}-LOV543wt/m3–WH1 chimeras was studied by saturating with blue LEDs illumination (30,000 lux; Fig. S2) for 10 min 600 μL protein solutions (3 μM wt and 5 μM m3) that were displayed in quartz

Fig. 7. Expression of LOV2–WH1–mCherry in *E. coli*. (a) Bacterial cells (DIC) with the intrinsic mCherry (red) and extrinsic ThS (cyan) fluorescence overlaid. Arrows point to intracellular aggregates. Right hand panels display the intensities of the ThS channel for the indicated linear traces. (b) Histogram showing the fraction of the cells in (a) carrying or not ThS-labeled aggregates. A control of cells expressing LOV2–mCherry under the same conditions (Fig. S8) is also displayed. The experiment was independently repeated three times. For each replica, 200 cells were counted, both under dark or blue light conditions. Bars represent SD from the mean values. Statistical significance analysis was performed with a Student's *t* test (95% confidence, ***$p < 0.001$, **$p < 0.01$, *$p < 0.1$). More bacteria accumulate amyloid aggregates (and these are larger) in the darkness than under blue light. (c) Scatter plot displaying the distribution of cell length for bacteria in panels a and b. Yellow segments: mean values. Red bars: SDs. Student's *t* test (95% confidence, ****$p < 0.0001$). The expression of LOV2–WH1–mCherry in the darkness results in a significant tendency to increase cell length. (d) Fractionation of bacterial lysates. Proteins were analyzed by SDS-PAGE (left) and Western-blotted with an anti–mCherry antibody (middle). (–), uninduced cells. Quantitation of the three culture replicas indicated that blue light illumination increases the solubility of the triple chimera. Student's *t* test (95% confidence, **$p < 0.01$, *$p < 0.1$). (e) Serial dilutions of cultures on agar plates show no significant inhibition of bacterial growth by blue light itself (left). Expression of LOV2–WH1–mCherry results in smaller colony sizes and in $\geq 10^2$-fold inhibition in the case of blue light illumination (right). (f) Growth curves of bacteria in liquid cultures expressing (IPTG-induced) LOV2–WH1–mCherry, or the control LOV2–mCherry, in the darkness and under blue light illumination. The experiment was performed in triplicate (bars: SDs). The inhibitory effect of expression of LOV2–WH1–mCherry under blue light observed in panels e and f is dependent on WH1, since it was not found for LOV2–mCherry.

cuvettes (1-cm path length) placed into the sample holder of an Ultrospec 3300pro spectrophotometer (GE Healthcare). To measure the return of excited flavin chromophore to the dark state [34,39], immediately after switching the light off, time-lapsed spectra acquisition started under the control of the Swift II software, with the following parameters: 300- to 600-nm wavelength interval (0.5 nm/data point), 2649-nm/min scan speed, and 24 consecutive spectra (i.e., one every 15 s). For the H_{10}-LOV543m3–WH1–mCherry chimera (8 μM), wavelength acquisition interval was extended to 650 nm to get the full band from excitation of mCherry. Return to the dark state was analyzed by fitting (MATLAB, The MathWorks Inc., release 2010a) a bi-exponential Levenberg–Marquardt function (R^2 = 0.9941 wt, 0.9771 m3, 0.9929 mCherry) to the A_{447nm} data points, corresponding to the main dark-state absorption band in LOV2.

For determining the association state of the chimeras, besides SEC (100 μL samples, 50 μM; see above), sedimentation velocity experiments were performed in a Beckman–Coulter Optima XL-I analytical ultracentrifuge, at 48,000 rpm and 20 °C, with 5 μM (H_{10}-LOV543m3–WH1) or 8 μM (H_{10}-LOV543m3–WH1–mCherry) protein in SEC buffer. Duplicates of each sample were displayed in two centrifuge cells, one of them was radially scanned (30-s intervals) at 275 nm (for the double chimera) or 590 nm (triple chimera) as the pseudo-dark state, and the other was scanned at 450 nm as the lit state. Continuous sedimentation coefficients distributions, $c(s)$, were fitted to the Lamm equation with SEDFIT [52] (Fig. S6).

CD spectroscopy was performed in a Jasco 720 spectropolarimeter, with 150 μL (2.5 μM) of each protein in SEC buffer. Samples were set in 0.1-cm path length quartz cuvettes held at 20 °C, and 7 spectra were acquired, in the darkness, at 50 nm min^{-1} and accumulated for signal averaging. Protein stability was estimated by thermal denaturation, measuring the variation of ellipticity (θ) at 220 nm with the increase of temperature (20–90 °C).

Limited proteolysis

Aliquots of purified H_{10}-LOV543wt–WH1 (3 μg) were diluted in 15 μL of SEC buffer including trypsin (0.025 units), chymotrypsin (0.004 u) or V8 (0.05 u) proteases (Sigma). Digestions proceeded for 1 and 2 h at RT, either in the darkness or under blue light illumination (30,000 lux; Fig. S2), and then stopped by adding SDS-PAGE loading buffer, followed by boiling and electrophoresis (12.5% polyacrylamide gels) and Coomassie blue staining. Replicated samples of the chymotrypsin and V8 digestions (1 h, blue light) were immediately frozen and transferred to the Protein Chemistry facility at CIB-CSIC for Edman's N-terminal sequencing (5 cycles in a Procise 494 sequencer; Applied Biosystems). In addition, the major bands resolved by SDS-PAGE were excised and trypsinized in-gel, and peptide fingerprinting of de-salted samples was performed by MALDI-TOF/TOF mass spectrometry (Autoflex III, Bruker) at the CIB-CSIC Proteomics facility. Peptides were assigned to the LOV543–WH1 sequence using the Mascot search engine (Matrix Science).

Optogenetic seeding of RepA-WH1(A31V) amyloidogenesis *in vitro*

Amyloidogenesis assays *in vitro* were carried out as described [51]. Two-milliliter Eppendorf tubes were set-up with 50 μL of 25 μM RepA-WH1(A31V) in fibril assembly buffer [0.1 M Na_2SO_4, 4 mM $MgSO_4$, 20 mM Hepes·NaOH (pH 8.0), 7% PEG4000, 3% 2-methyl-2,4-pentanediol]. Sub-stoichiometric amounts (1:100) of purified H_{10}-LOV543wt/m3–WH1 chimeras were used as seeds. Samples un-seeded or including RepA-WH1(A31V)–mCherry aggregated nuclei (0.1 μg) were also casted. Tubes were covered with aluminum foil or a thin PVC film, respectively, to avoid or allow illumination while preventing evaporation. Incubation proceeded under continuous shaking (300 rpm, 25 °C for 3 h) in a thermomixer (Eppendorf), either in the darkness or illuminating with blue light (30,000 lux; Fig. S2). Two-microliter aliquots were then immediately diluted in water (1:10), blotted to carbon-coated copper grids (400 mesh; EM Sciences) for negative staining with 2% uranyl acetate, and visualized in a JEOL JEM-1230 electron microscope (100 kV).

For amyloid probing, 5-μL sample aliquots were incubated with 200 μL of a ThS (0.05% w/v in 12.5 ethanol) for 30 min at RT and centrifuged (16,100*g*, 1 h at 4 °C), and the pellets washed twice with 200 μL of PBS buffer [53]. Aggregates were gently resuspended in 5 μL PBS and dried on glass slides. Samples were inspected in a Nikon Eclipse 90i epifluorescence microscope using 40× Plan Fluor objective (NA = 0.75) and a FITC filter (λ_{ex} = 482/35; λ_{em} = 536/40; exposure: 1 s). In parallel, 2-μL aliquots were incubated on glass slides with 2 μL of a saturated solution of CR in 70% ethanol. Apple-green birefringence was observed in a stereomicroscope (Leica $MZ12_5$) working at 3.2× magnification and with its two linear polarizers crossed at 90°.

Assessing H_{10}-LOV543m3–WH1–mCherry liquid–hydrogel phase transition *in vitro*

Forty microliters of samples were assembled in Eppendorf tubes under blue light (30,000 lux; Fig. S2), including LOV543m3–WH1–mCherry (250 μM) in 0.5× SEC buffer, 0.008% ThS, 9% PEG4000, and 4% 2-methyl-2,4-pentanediol.

After 2-h illumination at RT, tubes were transferred to the darkness and incubated overnight. Two microliters of each type of sample were pipetted, stained with uranyl acetate, and observed by TEM (see above). Ten microliters of drops were casted in parallel on glass slides under blue light illumination, immediately layered with a cover slip and then sealed with nail polish to avoid evaporation. Samples were kept under blue light at the epifluorescence microscope setting for 1 h, and then light was switched off and incubation proceeded for up to 24 h. A control sample was continuously illuminated for the same time interval. Epifluorescence was examined at the indicated time intervals in a Nikon Eclipse 90i microscope, using a 60× Plan Apo oil immersion objective (NA = 0.95) and TRITC (λ_{ex} = 543/22; λ_{em} = 593/40; exposure: 0.5 s) and cyan (λ_{ex} = 438/24; λ_{em} = 483/32; exp.: 0.3 s) filters. Differential interference contrast (DIC) images were also acquired (exp.: 0.3 s).

Optogenetic switching of H_{10}-LOV543m3–WH1–mCherry amyloidogenesis *in vivo*

E. coli MDS42 cultures carrying either pRK2-LOV543m3–WH1–mCherry or pRK2-*LOV543m3*–mCherry (Fig. S7) were grown in 100 mL of LB plus Ap_{100} in the darkness at 37 °C to OD_{600nm} = 0.2. Cultures were split into two 45-mL aliquots and placed in sterile bottles with a magnetic bar. IPTG was added (0.5 mM) to the 45 mL cultures (see above), and one of the flasks was covered with aluminum foil while the other was left unwrapped. Incubation under blue light or in the darkness proceeded for 4 h (37 °C, 150 rpm). Cells from 15 mL of the cultures were harvested and washed twice with PBS. Pellets were resuspended in 1 mL of PBS and, while 0.9 mL was centrifuged and cells were stored at −70 °C for solubility tests, bacteria from the other 0.1 mL were fixed with 4% paraformaldehyde (Sigma) [51]. Fixed cells were stained with ThS, displayed on glass slides, and mounted with Fluoromount-G (SouthernBiotech) before observation in a Nikon Eclipse 90i microscope (see above), using a 100× Plan Apo oil immersion objective (NA = 1.4).

For assessing the effect of the expression of the optogenetic device on bacterial growth, cultures carrying pRK2-LOV543m3–WH1–mCherry or pRK2-*LOV543m3*–mCherry were left to grow to OD_{600nm} = 1.0, when serial dilutions (7 μL drops) were spotted on LB-agar plus Ap_{100} ± 1.0 mM IPTG and incubated for 30 h at 37 °C, either in the darkness or under blue light (1070 lux; Fig. S2). Independently, preinocula of the same bacterial strains grown in the darkness in LB plus Ap_{100} were inoculated (starting OD_{600nm} = 0.01) in triplicate in 20 mL of LB supplemented with Ap_{100} and 0.5 mM IPTG. Cultures were then grown either in the darkness or under blue light illumination, as indicated above. Measurements of OD_{600nm} were acquired at intervals of 1 h for 15 h.

CRediT authorship contribution statement

Rafael Giraldo: Conceptualization, Funding acquisition, Investigation, Methodology, Writing - original draft, Writing - review & editing.

Acknowledgments

This article is dedicated to the memory of Aaron Klug (1926-2018). The author thanks his group for encouragement and patience during the years invested in this work. The members of the CIB-CSIC workshop Aurelio Hurtado, Alejandro Ayuda and Ángel Atienza are much appreciated for the construction of the LED light source. Thanks are due to Ana Serrano for help with site-directed mutagenesis and to the CIB-CSIC staff members Juan R. Luque (analytical ultracentrifugation), Javier Varela (N-terminal peptide sequencing), and Francisco García-Tabares and Vivian de los Ríos (peptide fingerprinting). Carlos Fernández-Tornero is acknowledged for access to the stereomicroscope used in the CR assay. The author is grateful to Douglas Laurents for the critical reading of an early version of the manuscript. This work has been financed with grants from the Spanish AEI (BIO2012-30852 and BIO2015-68730-R).

Author Contributions: R.G. conceived the project, carried out the experimental work, analyzed data, and wrote the manuscript.

Competing Interests: R.G. is the inventor of a patent (EP18382882) deposited by CSIC on the optogenetic devices described here.

Appendix A. Supplementary data

Supplementary data to this article can be found online at https://doi.org/10.1016/j.jmb.2019.01.037.

Received 16 October 2018;
Received in revised form 24 January 2019;
Accepted 28 January 2019
Available online 2 February 2019

Keywords:
LOV2;
optobiotics;
phase transitions;
prion-like;
RepA-WH1

Abbreviations used:
CD, circular dichroism; CR, Congo red: 3,3′-([1,1′-biphenyl]-4,4′-diyl)bis(4-aminonaphthalene-1-sulfonate); IDRs, intrinsically disordered regions; LED, light-emitting diode; LOV2, light-oxygen-voltage 2; PEG, polyethylene glycol; SEC, size-exclusion chromatography; TEM, transmission electron microscopy; ThS, thioflavin S; WH, winged-helix.

References

[1] D.S. Eisenberg, M.R. Sawaya, Structural studies of amyloid proteins at the molecular level, Annu. Rev. Biochem. 86 (2017) 69–95, https://doi.org/10.1146/annurev-biochem-061516-045104.

[2] T. Eichner, S.E. Radford, A diversity of assembly mechanisms of a generic amyloid fold, Mol. Cell 43 (2011) 8–18, https://doi.org/10.1016/j.molcel.2011.05.012.

[3] S. Alberti, S. Saha, J.B. Woodruff, T.M. Franzmann, J. Wang, A.A. Hyman, A user's guide for phase separation assays with purified proteins, J. Mol. Biol. 430 (2018) 4806–4820, https://doi.org/10.1016/j.jmb.2018.06.038.

[4] S. Maharana, J. Wang, D.K. Papadopoulos, D. Richter, A. Pozniakovsky, I. Poser, M. Bickle, S. Rizk, J. Guillén-Boixet, T.M. Franzmann, M. Jahnel, L. Marrone, Y.T. Chang, J. Sterneckert, P. Tomancak, A.A. Hyman, S. Alberti, RNA buffers the phase separation behavior of prion-like RNA binding proteins, Science 360 (2018) 918–921, https://doi.org/10.1126/science.aar7366.

[5] C.P. Brangwynne, C.R. Eckmann, D.S. Courson, A. Rybarska, C. Hoege, J. Gharakhani, F. Jülicher, A.A. Hyman, Germline P granules are liquid droplets that localize by controlled dissolution/condensation, Science 324 (2009) 1729–1732, https://doi.org/10.1126/science.1172046.

[6] E.M. Courchaine, A. Lu, K.M. Neugebauer, Droplet organelles? EMBO J. 35 (2016) 1603–1612, https://doi.org/10.15252/embj.201593517.

[7] Y. Shin, C.P. Brangwynne, Liquid phase condensation in cell physiology and disease, Science 357 (2017), eaaf4382. https://doi.org/10.1126/science.aaf4382.

[8] S. Boeynaems, S. Alberti, N.L. Fawzi, T. Mittaq, N. Polymenidou, F. Rousseau, J. Schymkowitz, J. Shorter, D. Wolozin, L. Van Den Bosch, P. Tompa, M. Fuxreiter, Protein phase separation: a new phase in cell biology, Trends Cell Biol. 28 (2018) 420–435, https://doi.org/10.1016/j.tcb.2018.02.004.

[9] R. Giraldo, C. Fernández-Tornero, P.R. Evans, R. Díaz-Orejas, A. Romero, A conformational switch between transcriptional repression and replication initiation in the RepA dimerization domain, Nat. Struct. Biol. 10 (2003) 565–571, https://doi.org/10.1038/nsb937.

[10] L. Molina-García, F. Gasset-Rosa, M. Moreno-del Álamo, M.E. Fernández-Tresguerres, S. Moreno-Díaz de la Espina, R. Lurz, R. Giraldo, Functional amyloids as inhibitors of plasmid DNA replication, Sci. Rep. 6 (2016) 25425, https://doi.org/10.1038/srep25425.

[11] R. Giraldo, Defined DNA sequences promote the assembly of a bacterial protein into distinct amyloid nanostructures, Proc. Natl. Acad. Sci. U. S. A. 104 (2007) 17388–17393, https://doi.org/10.1073/pnas.0702006104.

[12] F. Gasset-Rosa, M.J. Maté, C. Dávila-Fajardo, J. Bravo, R. Giraldo, Binding of sulphonated indigo derivatives to RepA-WH1 inhibits DNA-induced protein amyloidogenesis, Nucleic Acids Res. 36 (2008) 2249–2256, https://doi.org/10.1093/nar/gkn067.

[13] M. Moreno-del Álamo, S. Moreno-Díaz de la Espina, M.E. Fernández-Tresguerres, R. Giraldo, Pre-amyloid oligomers of the proteotoxic RepA-WH1 prionoid assemble at the bacterial nucleoid, Sci. Rep. 5 (2015) 14669, https://doi.org/10.1038/srep14669.

[14] C. Fernández, R. Núñez-Ramírez, M. Jiménez, G. Rivas, R. Giraldo, RepA-WH1, the agent of an amyloid proteinopathy in bacteria, builds oligomeric pores through lipid vesicles, Sci. Rep. 6 (2016) 23144, https://doi.org/10.1038/srep23144.

[15] M.E. Fernández-Tresguerres, S. Moreno-Díaz de la Espina, F. Gasset-Rosa, R. Giraldo, A DNA-promoted amyloid proteinopathy in *Escherichia coli*, Mol. Microbiol. 77 (2010) 1456–1469, https://doi.org/10.1111/j.1365-2958.2010.07299.x.

[16] F. Gasset-Rosa, A.S. Coquel, M. Moreno-del Álamo, P. Chen, X. Song, A.M. Serrano, S. Moreno-Díaz de la Espina, A.B. Lindner, R. Giraldo, Direct assessment in bacteria of prionoid propagation and phenotype selection by Hsp70 chaperone, Mol. Microbiol. 91 (2014) 1070–1087, https://doi.org/10.1111/mmi.12518.

[17] L. Molina-García, M. Moreno-del Álamo, P. Botias, Z. Martín-Moldes, M. Fernández, A. Sánchez-Gorostiaga, A. Alonso-del Valle, J. Nogales, J. García-Cantalejo, R. Giraldo, Outlining core pathways of amyloid toxicity in bacteria with the RepA-WH1 prionoid, Front. Microbiol. 8 (2017) 539, https://doi.org/10.3389/fmicb.2017.00539.

[18] C. Fernández, G. González-Rubio, J. Langer, G. Tardajos, L. M. Liz-Marzán, R. Giraldo, A. Guerrero-Martínez, Nucleation of amyloid oligomers by RepA-WH1 prionoid-functionalized gold nanorods, Angew. Chem. Int. Ed. 55 (2016) 11237–11241, https://doi.org/10.1002/anie.201604970.

[19] F. Gasset-Rosa, R. Giraldo, Engineered bacterial hydrophobic oligopeptide repeats in a synthetic yeast prion, [*REP-PSI*$^{+}$], Front. Microbiol. 6 (2015) 311, https://doi.org/10.3389/fmicb.2015.00311.

[20] L. Molina-García, R. Giraldo, Enabling stop codon read-through translation in bacteria as a probe for amyloid aggregation, Sci. Rep. 7 (2017) 11908, https://doi.org/10.1038/s41598-017-12174-0.

[21] J.S. Khamo, V.V. Krishnamurthy, S.R. Sharum, P. Mondal, K. Zhang, Applications of optobiology in intact cells and multicellular organisms, J. Mol. Biol. 429 (2017) 2999–3017, https://doi.org/10.1016/j.jmb.2017.08.015.

[22] B.R. Rost, F. Schneider-Warme, D. Schmitz, P. Hegemann, Optogenetic tools for subcellular applications in neuroscience, Neuron 96 (2017) 572–603, https://doi.org/10.1016/j.neuron.2017.09.047.

[23] A. Möglich, X. Yang, R.A. Ayers, K. Moffat, Structure and function of plant photoreceptors, Annu. Rev. Plant Biol. 61 (2010) 21–47, https://doi.org/10.1146/annurev-arplant-042809-112259.

[24] A. Pudasaini, K. El-Arab, B.D. Zoltowski, LOV-based optogenetic devices: light-driven modules to impart photoregulated control of cellular signalling, Front. Mol. Biosci. 2 (2015) 18, https://doi.org/10.3389/fmolb.2015.00018.

[25] S.P. Zimmerman, B. Kuhlman, H. Yumerefendi, Engineering and applications of LOV2-based photoswitches, Methods Enzymol. 580 (2016) 169–190, https://doi.org/10.1016/bs.mie.2016.05.058.

[26] A. Möglich, K. Moffat, Engineered photoreceptors as novel optogenetic tools, Photochem. Photobiol. Sci. 9 (2010) 1286–1300, https://doi.org/10.1039/c0pp00167h.

[27] Y. Shin, J. Berry, N. Pannucci, M.P. Haataja, J.E. Toettcher, C.P. Brangwynne, Spatiotemporal control of intracellular

phase transitions using light-activated optoDroplets, Cell 168 (2017) 159–171, https://doi.org/10.1016/j.cell.2016.11.054.
[28] D. Bracha, M.T. Walls, M.T. Wei, L. Zhu, M. Kurian, J.L. Avalos, J.E. Toettcher, C.P. Brangwynne, Mapping local and global liquid phase behavior in living cells using photo-oligomerizable seeds, Cell 175 (2018) 1467–1480, https://doi.org/10.1016/j.cell.2018.10.048.
[29] A.S. Halavaty, K. Moffat, N- and C-terminal flanking regions modulate light-induced signal transduction in the LOV2 domain of the blue light sensor phototropin 1 from *Avena sativa*, Biochemistry 46 (2007) 14001–14009, https://doi.org/10.1021/bi701543e.
[30] S.M. Harper, L.C. Neil, K.H. Gardner, Structural basis of a phototropin light switch, Science 301 (2003) 1541–1544, https://doi.org/10.1126/science.1086810.
[31] A.I. Nash, W.H. Ko, S.M. Harper, K.H. Gardner, A conserved glutamine plays a central role in LOV domain signal transmission and its duration, Biochemistry 47 (2008) 13842–13849, https://doi.org/10.1021/bi801430e.
[32] D. Strickland, K. Moffat, T.R. Sosnick, Light-activated DNA binding in a designed allosteric protein, Proc. Natl. Acad. Sci. U. S. A. 105 (2008) 10709–10714, https://doi.org/10.1073/pnas.0709610105.
[33] D. Strickland, X. Yao, G. Gawlak, M.L. Rosen, K.H. Gardner, T.R. Sosnick, Rationally improving LOV domain-based photoswitches, Nat. Methods 7 (2010) 623–626, https://doi.org/10.1038/nmeth.1473.
[34] J. Zayner, T.R. Sosnick, Factors that control the chemistry of the LOV domain photocycle, PLoS One 9 (2014), e87074. https://doi.org/10.1371/journal.pone.0087074.
[35] L. Molina-García, R. Giraldo, Aggregation interplay between variants of the RepA-WH1 prionoid in *Escherichia coli*, J. Bacteriol. 196 (2014) 2536–2542, https://doi.org/10.1128/JB.01527-14.
[36] A. Vallée-Bélisle, F. Ricci, K.W. Plaxco, Thermodynamic basis for the optimization of binding-induced biomolecular switches and structure-switching biosensors, Proc. Natl. Acad. Sci. U. S. A. 106 (2009) 13802–13807, https://doi.org/10.1073/pnas.0904005106.
[37] O.I. Lungu, R.A. Hallett, E.J. Choi, M.J. Aiken, K.M. Hahn, B. Kuhlman, Designing photoswitchable peptides using the AsLOV2 domain, Chem. Biol. 19 (2012) 507–517, https://doi.org/10.1016/j.chembiol.2012.02.006.
[38] C.A. Rohl, C.E. Strauss, K.M. Misura, D. Baker, Protein structure prediction using Rosetta, Methods Enzymol. 383 (2004) 66–93, https://doi.org/10.1016/S0076-6879(04)83004-0.
[39] B.D. Zoltowski, B. Vaccaro, B.R. Crane, Mechanism-based tuning of a LOV domain photoreceptor, Nat. Chem. Biol. 5 (2009) 827–834, https://doi.org/10.1038/nchembio.210.
[40] M.C. Manning, R.W. Woody, Theoretical CD studies of polypeptide helices: examination of important electronic and geometric factors, Biopolymers 31 (1991) 569–586, https://doi.org/10.1002/bip.360310511.
[41] E. Torreira, M. Moreno-del Álamo, M.E. Fuentes-Perez, C. Fernández, J. Martín-Benito, F. Moreno-Herrero, R. Giraldo, O. Llorca, Amyloidogenesis of bacterial prionoid RepA-WH1 recapitulates dimer to monomer transitions of RepA in DNA replication initiation, Structure 23 (2015) 183–189, https://doi.org/10.1016/j.str.2014.11.007.
[42] S.T. Glantz, E.J. Carpenter, M. Melkonian, K.H. Gardner, E.S. Boyden, G.K.S. Wong, B.Y. Chow, Functional and topological diversity of LOV domain photoreceptors, Proc. Natl. Acad. Sci. U. S. A. 113 (2016) E1442–E1451, https://doi.org/10.1073/pnas.1509428113.
[43] B.R. Parry, I.V. Surovtsev, M.T. Cabeen, C.S. O'Hern, E.R. Dufresne, C. Jacobs-Wagner, The bacterial cytoplasm has glass-like properties and is fluidized by metabolic activity, Cell 156 (2014) 183–194, https://doi.org/10.1016/j.cell.2013.11.028.
[44] D. Mateju, T.M. Franzmann, A. Patel, A. Kopach, E.E. Boczek, S. Maharana, H.O. Lee, S. Carra, A.A. Hyman, S. Alberti, An aberrant phase transition of stress granules triggered by misfolded protein prevented by chaperone function, EMBO J. 36 (2017) 1669–1697, https://doi.org/10.15252/embj.201695957.
[45] H.X. Zhou, V. Nguemaha, K. Mazarakos, S. Qin, Why do disordered and structured proteins behave differently in phase separation? Trends Biochem. Sci. 43 (2018) 499–2516, https://doi.org/10.1016/j.tibs.2018.03.007.
[46] R. Giraldo, Amyloid assemblies: protein legos at a crossroads in bottom-up synthetic biology, Chembiochem 11 (2010) 2347–2357, https://doi.org/10.1002/cbic.201000412.
[47] Y. Wang, J. Pu, B. An, T.K. Lu, C. Zhong, Emerging paradigms for synthetic design of functional amyloids, J. Mol. Biol. 430 (2018) 3720–3734, https://doi.org/10.1016/j.jmb.2018.04.012.
[48] M. Moreno-del Alamo, A. Sánchez-Gorostiaga, A.M. Serrano, A. Prieto, J. Cuéllar, J. Martín-Benito, J.M. Valpuesta, R. Giraldo, Structural analysis of the interactions between Hsp70 chaperones and the yeast DNA replication protein Orc4p, J. Mol. Biol. 403 (2010) 24–39, https://doi.org/10.1016/j.jmb.2010.08.022.
[49] E. Martínez-García, T. Aparicio, A. Goñi-Moreno, S. Fraile, V. de Lorenzo, SEVA 2.0: An update of the standard European vector architecture for de–/re-construction of bacterial functionalities, Nucleic Acids Res. 28 (2015) D1183–D1189, https://doi.org/10.1093/nar/gku1114.
[50] G. Pósfai, G. Plunkett III, T. Fehér, D. Frisch, G.M. Keil, K. Umenhoffer, V. Kolisnychenko, B. Stahl, S.S. Sharma, M. de Arruda, V. Burland, S.W. Harcum, F.R. Blattner, Emergent properties of reduced-genome *Escherichia coli*, Science 312 (2006) 1044–1046, https://doi.org/10.1126/science.1126439.
[51] L. Molina-García, F. Gasset-Rosa, M. Moreno-del Álamo, S. Moreno-Díaz de la Espina, R. Giraldo, Addressing intracellular amyloidosis in bacteria with RepA-WH1, a prion-like protein, Methods Mol. Biol. 1779 (2018) 289–312, https://doi.org/10.1007/978-1-4939-7816-8_18.
[52] P. Schuck, Size-distribution analysis of macromolecules by sedimentation velocity ultracentrifugation and Lamm equation modelling, Biophys. J. 78 (2000) 1606–1619, https://doi.org/10.1016/S0006-3495(00)76713-0.
[53] P. Aguilera, A. Marcoleta, P. Lobos-Ruiz, R. Arranz, J.M. Valpuesta, O. Monasterio, R. Lagos, Identification of key amino acid residues modulating intracellular and *in vitro* microcin E492 amyloid formation, Front. Microbiol. 7 (2016) 35, https://doi.org/10.3389/fmicb.2016.00035.